Journal of Applied Electrochemistry (2007) 37:49–55
DOI 10.1007/s10800-006-9213-0

Electrodiffusion diagnostics of the flow and mass transfer inside a network of crossing minichannels

F. HUCHET[1], J. COMITI[1,*], J. TIHON[2], A. MONTILLET[1] and P. LEGENTILHOMME[1]
[1]*Laboratoire de Génie des Procédés, Environnement, Agroalimentaire, GEPEA UMR CNRS 6144, C.R.T.T, 37 Bd de l'Université, BP 406, 44602, Saint-Nazaire-Cedex, France*
[2]*Institute of Chemical Process Fundamentals, Academy of Sciences of the Czech Republic, Rozvojová 135, 16502, Prague 6, Czech Republic*
*(*author for correspondence, tel.: + 33-240172632, fax: + 33-240172618, e-mail: jacques.comiti@univ-nantes.fr)*

Received 14 February 2006; accepted in revised form 3 April 2006

Key words: crossing minichannels, electrodiffusion technique, flow diagnostics, flow regimes, mass transfer, wall shear rate

Abstract

The global mass transfer and the local flow structure inside a set of crossing minichannels were characterized using the electrodiffusion method. The individual square-cross channel sections ($a = 1.5$ mm in sides) intersect at right-angles in order to form the flow cell. An array of 39 circular platinum electrodes (0.25 mm in diameter) was flush-mounted into the wall of the flow cell to investigate the wall shear rate at different locations. This array of small sensors allowed characterization of longitudinal and lateral variations in wall shear rate across the flow cell, flow distribution at the inlet and outlet sections, transition between laminar and turbulent flow regimes, and flow behaviour at the channel crossings. The results of global wall mass transfer measurements demonstrated that, from a mass transfer point of view, the flow cell exhibits similar behaviour to a porous medium.

1. Introduction

The study of microfluidic systems is now an important research challenge related to microdevices in chemical processes. The understanding of physical phenomena, such as, for example, the transition between laminar and turbulent flow regimes is very important for industrial applications. The miniaturization of industrial equipment such as mixers, reactors or heat and mass exchangers is a new approach for process engineering [1, 2]. The aim is to increase heat and mass transfer due to an enhanced ratio between surface and volume. The goal is to connect a set of components of different sizes to form network units and thus produce new multiscale plants. Characterization of the flow behaviour and heat and mass transfer performance is needed in order to develop these micro or minisystems.

Several papers deal with flow through minichannels of different shapes. Most of them have been summarized in a review by Morini [3], which emphasizes that experimental results concerning the friction factors and heat transfer rates in microtubes are relatively scattered. Several authors [4, 5] measured values of friction factor greater than those normally expected in laminar flow. This scatter could be explained by the nature of the fluids and the differences in geometry and surface roughness.

This work is dedicated to the determination of flow regimes in a special flow cell consisting of crossing minichannels. The electrodiffusion probes are used for the mapping of wall shear rates in the flow cell. An array of 39 microelectrodes allows us to characterize the transition between the laminar and turbulent flow regimes, longitudinal and lateral distributions of wall shear rate across the flow cell, flow distribution at the inlet and outlet sections and flow behaviour at the channel crossings. The electrodiffusion diagnostics of the flow are completed by a liquid-solid mass transfer study performed at three large nickel electrodes.

2. Electrodiffusion technique

The electrodiffusion technique using small probes flush-mounted in the wall is often used to measure local values of wall shear rate [6]. The probe active surface works as a small electrode where a fast electrochemical reaction takes place. The mean measured limiting current $\overline{I}$ is controlled by convective diffusion and the well-known Lévêque formula can be applied to determine the mean wall shear rate $\overline{s}$

$$\overline{I} = 0.677 n F c_0 d^{5/3} D^{2/3} \overline{s}^{1/3}, \quad (1)$$

where n is the number of electrons involved in the electrochemical reaction, F is the Faraday constant, d is the diameter of a circular electrode, c_0 is the bulk concentration of the active ions, and D is their diffusivity in the solution. The reduction of ferricyanide ions on a platinum cathode ($Fe(CN)_6^{3-} + e^- \rightarrow Fe(CN)_6^{4-}$) is the most popular electrochemical reaction used for such flow diagnostics.

The instantaneous values of wall shear rate $s(t)$ can be directly related to the measured values of limiting diffusion current $I(t)$ only if the assumption of slow flow fluctuations is fulfilled. Under highly unsteady flow conditions, the frequency response of electrodiffusion probes has to be taken into account. The correction in respect to probe dynamic behaviour can be done in the frequency domain. The transfer function $H(f)$, suggested for circular electrodiffusion probes [7], enables the recovery of the frequency spectrum of shear rate fluctuations $W_{ss}(f)$ from the current fluctuation spectrum $W_{ii}(f)$

$$W_{ss}(f) = |H(f)|^2 W_{ii}(f). \quad (2)$$

This relationship was found to be suitable even at high flow fluctuations frequencies [8].

The electrodiffusion method can also be applied to the determination of mass transfer at the wall. In this case, an electrode with a large active surface A is used and the global mass transfer coefficient k_{mt} is related to the mean limiting diffusion current $\overline{I}$ by the simple formula

$$k_{mt} = \overline{I}/(nFc_o A), \quad (3)$$

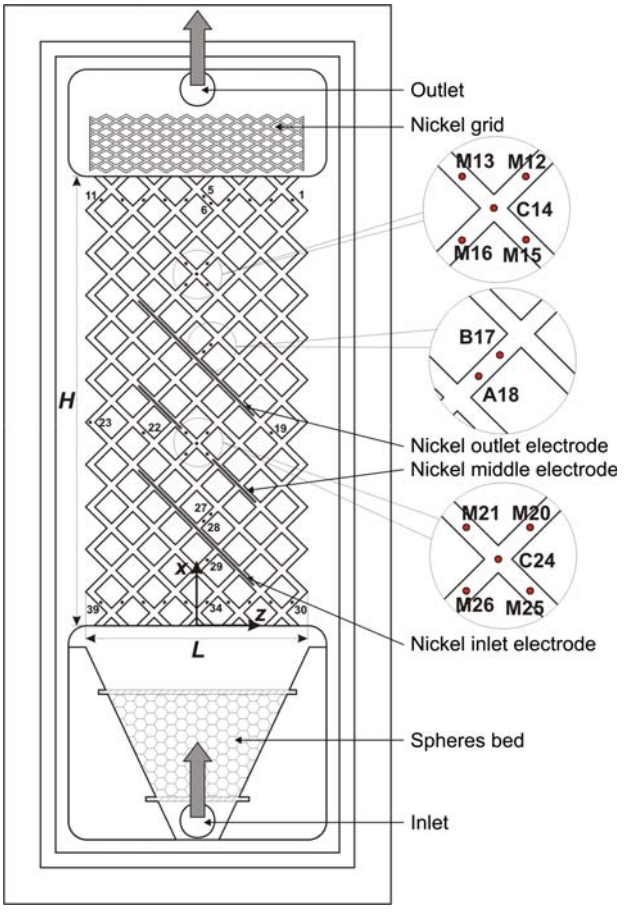

Fig. 1. Scheme of the experimental cell.

3. Description of the experiments

3.1. *Experimental equipment*

The experimental cell is shown in Figure 1. It was made of Altuglas and featured crossing minichannels. The individual square-cross sections of the channels (1.5 × 1.5 mm) intersect at right angles. The whole test section had a length of $H = 105$ mm and a width of $W = 52$ mm. At the inlet, there was a calming section containing glass spheres 2 mm in diameter, which allowed better distribution of the fluid. Thirty nine circular platinum microelectrodes were flush-mounted into the upper wall of the flow cell. They had a nominal diameter of 0.25 mm and acted as cathodes. The anode was made of a nickel grid located at the cell outlet section. As seen in Figure 1, the microelectrodes were numbered from right to left and from top to bottom. The microelectrode positions with respect to the individual minichannel sections were designated with four different labels: M (at the middle of a channel section), A (just after channel crossing), B (just before crossing), and C (at the centre of a channel crossing). Two dimensionless parameters were used to determine the position of each probe inside the network of minichannels. The axial position was represented by the parameter $X = x/H$ and the lateral one by $Z = 2z/L$. Large nickel electrodes (strips $l_e = 3.65$ mm in length and 1.5 mm in width) were placed at three flow cell positions in order to study the global mass transfer inside the flow cell. The exact surface area of each electrode was obtained by image analysis.

A suitable electrochemical system was provided by addition of 0.025 M equimolar potassium ferro/ferricyanide and 0.05 M potassium sulphate into water. A polarization voltage of −0.8 V was applied to ensure limiting diffusion current conditions. The experiments were performed at Reynolds numbers Re ranged from 50 to 3000. The Reynolds number, $Re = u_{ch} \cdot d_H/\nu$, is based on the mean velocity inside individual channel sections u_{ch}, the channel hydraulic diameter d_H, and the kinematic viscosity of the working fluid ν. All measurements were carried out at room temperature.

3.2. *Calibration of the microelectrodes*

The calibration technique used in this work was based on the study of the transient response of the microelectrode current to polarization switch-on [9, 10]. This current response is described by the well-known solution of unsteady diffusion in a stagnant fluid

$$I(t) = \frac{1}{4} nFc_0 \pi d^2 \sqrt{D/\pi t}. \quad (4)$$

The transient currents measured immediately after a step change of potential was firstly used to determine the temperature-dependent diffusivity of ferri/ferrocyanide ions. These measurements were performed with a large circular platinum probe (d = 2mm) in a vessel immersed in a thermostatic bath. The results were expressed in the form of the Stokes–Einstein relationship between dynamic viscosity μ, diffusivity D and absolute temperature T

$$\frac{\mu D}{T} \cong 2.18 \times 10^{-15} [\text{kg m s}^{-2}\,\text{K}^{-1}], \quad (5)$$

which is valid for the temperature range 285–305 K. The corresponding values of dynamic viscosity were measured using a rotation rheometer (Haake RS150). When the diffusivity was known, the same type of measurements was applied to provide information on the individual effective diameters, d_e, for all the microelectrodes. In spite of the shape deformation during the process of microelectrode fabrication, the effective diameter values were found to be close to the platinum wire nominal diameter (d=0.25 mm). This calibration procedure provided the values of D and d_e necessary for application of Equation (1).

3.3. *Data acquisition and treatment*

A home built electrodiffusion analyser was used to set the polarization voltage to the microelectrodes, to convert the measured currents into voltages, and to amplify the resulting signals. A PC computer controlled the analyser operation and data recording. Data records (ranging from 30,000 to 80,000 samples depending on Reynolds number) for eight current signals were provided at a sampling frequency ranging from 1 to 10 kHz. The measured signals were passed through a discrete fast Fourier transformation to obtain the power spectral densities of current fluctuation W_{ii}. Then the transfer function $H(f)$ (see Equation (2)) was applied to obtain the power spectral densities of wall shear rate fluctuations W_{ss} and after spectra integration to access the fluctuating rates FR

$$FR = \sqrt{\overline{s'^2}}/\bar{s} = \sqrt{\int W_{ss} df}/\bar{s}, \text{ with } s(t) = \bar{s} + s'(t) \quad (6)$$

4. Results and discussion

4.1. *Characterization of the flow regimes*

An example of wall shear rate traces measured inside the flow cell is shown in Figure 2. For these measurements carried out near the cell outlet, the first flow fluctuations are observed at Re$\sim$200. As the flow rate increases, the level of fluctuations increases.

It is interesting to analyze the results obtained for the microelectrodes located at different axial positions. The fluctuation rates, FR, presented in Figure 3, illustrate the typical flow regimes achieved in the flow cell and also the gradual development of fluctuations along the cell. The variation of FR with Re is characterized by an initial plateau at $FR\sim0$ (laminar flow regime), then FR increases sharply (transient flow regime) up to a practically constant level (regime of developed flow

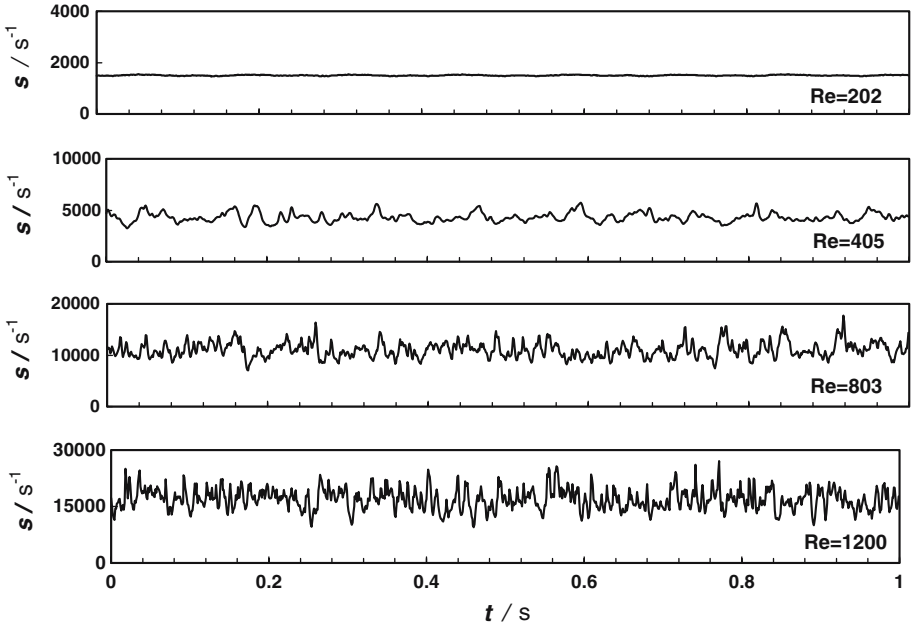

Fig. 2. Time traces of the wall shear rate measured at the electrode B5, which is located close to the cell outlet at the position of it X = 0.95, Z = 0.28.

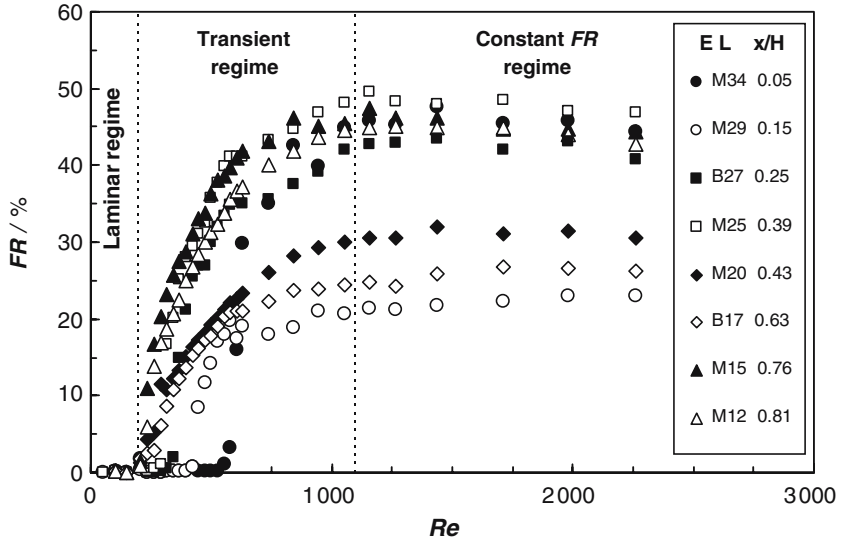

Fig. 3. Variations of fluctuation rates $FR = \sqrt{\overline{s'^2}}/\bar{s}$ with the Reynolds number obtained for the different axial locations $X = x/H$.

fluctuations), whose actual value depends on the specific probe location. The critical value of Re corresponding to the onset of fluctuations varies from 560 (for the probe M34 located close to the cell inlet) to 200 (for all the electrodes behind the third channel crossing). Therefore, the flow inside the network of channels can be considered as established for axial locations $X > 0.3$.

Only at low flow rates (for $Re < 200$), there is a stable laminar regime observed throughout the flow cell. On the other hand, stabilization of near-wall flow fluctuations occurs at high flow rates and is observed everywhere in the cell for $Re > 1100$. As the flow pattern is very complex (3D with recirculation zones behind the crossings), the final value of FR is very sensitive to the exact position of the microelectrode (especially with respect to the channel centreline). The fluctuation rates were found to stabilize at relative values ranging from 20 to 50%. The channel crossings have an effect on the enhancement of flow fluctuations and also on their earlier stabilization than in straight channels. The shape of FR vs Re curves is very similar to that observed for the evolution of fluctuations in packed beds of particles. The packed bed flow configurations also exhibit practically the same critical Re values characterizing the onset ($Re \sim 180$) and the stabilization ($Re \sim 900$) of flow fluctuations [11, 12].

The power spectra of wall shear rate fluctuations measured for several values of Reynolds number are compared in Figure 4. The spectra exhibit typical features of a turbulent spectrum: a plateau at low frequencies and a regular decline at high frequencies. However, the slope in the high-frequency region is generally higher than the value of $-5/3$, which characterizes isotropic turbulent flow conditions. Consequently, although the values of fluctuation rates are high and relatively stable at Re from 1100 to 3000, the

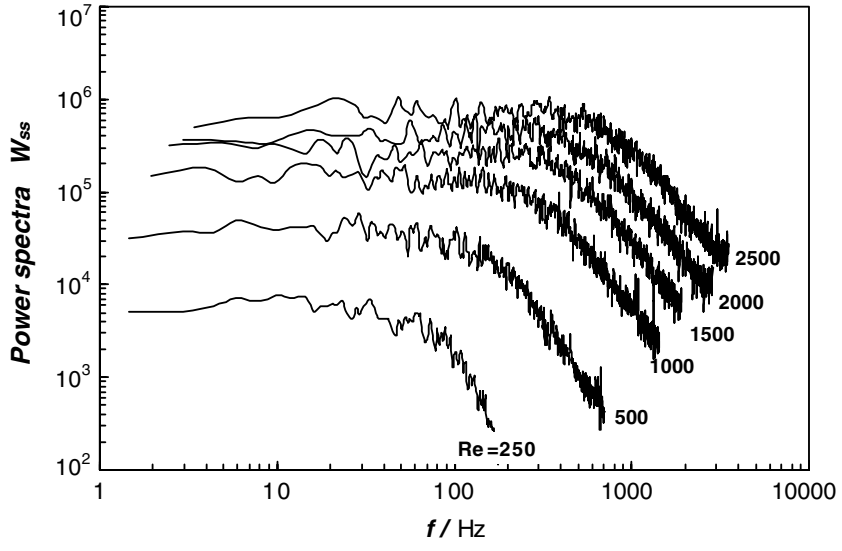

Fig. 4. Power spectra of wall shear rate fluctuations measured for the different Reynolds numbers at the location of the probe M12.

flow in crossing minichannels cannot be considered as a fully developed turbulent flow. That is why we use the term "fluctuation rate" instead of "turbulence intensity" for the description of flow unsteadiness. The wall shear rate data recorded by the other microelectrodes provided similar spectral results as that shown in Figure 4.

4.2. *Local flow structure*

The flow inside the cell is complex and unsteady, especially around the channel crossings. Some information on local flow structures can be extracted from the comparison of results obtained for four types of differently located microelectrodes.

4.2.1. *Flow structure in the middle of channel sections ("M" probes)*

To characterize the local flow in the middle of channel sections, Figure 5 presents the *FR* data for the "M" probes at $Re = 1200$. This flow rate is sufficient to reach the practically constant *FR* level at all the measuring locations. The values of *FR* are rather scattered around the mean value of *FR*∼42%. It suggests large local changes in the flow structure even though the flow distribution at the cell inlet was found to be uniform ($\bar{s} \sim 5100 s^{-1}$). Much less homogenous flow conditions were found at the cell outlet with $\bar{s}$ values ranging from 4,000 to 10,000 s^{-1}.

4.2.2. *Flow structure at channel crossings ("A, B, C" probes)*

Figure 6 shows typical wall shear rate results obtained for five microelectrodes situated at a channel crossing (M12, M13, C14, M15, M16). The microelectrode C14 located just at the crossing centre exhibits a much higher value of $\bar{s} \sim 15,000\,s^{-1}$ than those located at the middle channel sections providing values around $\bar{s} \sim 6,000\,s^{-1}$. The opposite trend can be seen for the fluctuation rate values, thus the higher $\bar{s}$ values at channel crossings are accompanied by lower *FR* values. The reduction of channel sections at crossings works like a Venturi

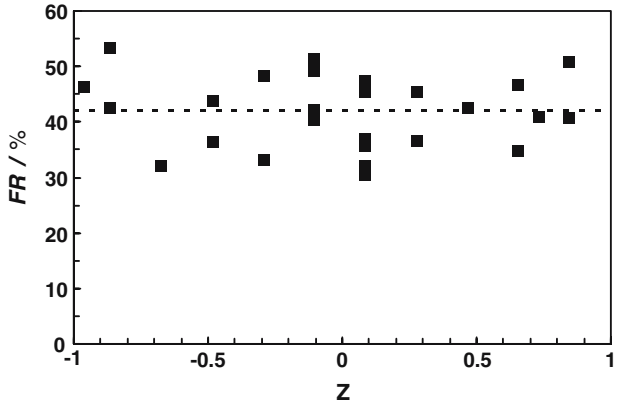

Fig. 5. Scatter of relative values of the fluctuation rates *FR* measured at the different "M" locations.

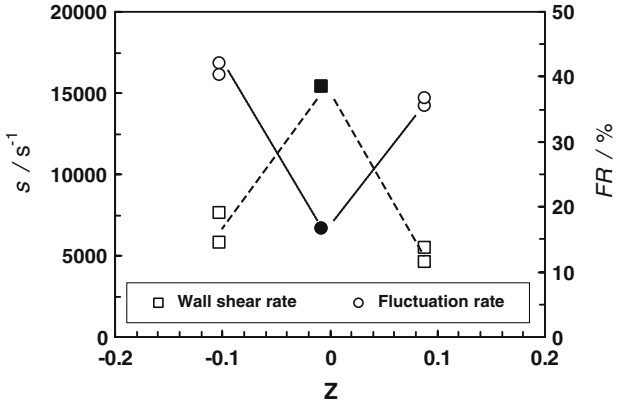

Fig. 6. Wall shear rate data measured at the channel crossing: M12, M13, M15, M16 (open symbols) and C14 (solid symbols).

throat. It means that the flow acceleration expected here enhances the wall shear rates and damps the flow fluctuations. Our recent PIV measurements carried out in the same flow configuration has confirmed that the flow observed at the crossing centres can be considered as plug flow.

The current signals measured close to the crossings at locations "A" and "B" provide generally lower values of *FR* than those corresponding to "M" probes. The flow in these locations is affected by calm regions or recirculation zones appearing in front of and behind the channel crossings.

4.3. *Liquid-solid mass transfer*

The experimental results on wall mass transfer obtained for three large electrodes are plotted in Figure 7. These data are represented in the dimensionless form $\mathrm{Sh}\,\mathrm{Sc}^{-1/3} = f(Re)$ by using the Sherwood ($\mathrm{Sh} = k_{\mathrm{mt}} d_h / D$), Schmidt ($\mathrm{Sc} = \nu / D$) and Reynolds numbers. If the results are presented in logarithmic coordinates, two almost linear regions can be distinguished. Two corresponding correlations cover almost the whole range of experimental data:

$$\mathrm{Sh}\,\mathrm{Sc}^{-1/3} = 0.94 Re^{0.41} \quad (\text{for } 15 < Re < 100,\ \text{laminar regime}) \tag{7}$$

and

$$\mathrm{Sh}\,\mathrm{Sc}^{-1/3} = 0.29 Re^{0.66} \quad (\text{for } 200 < Re < 3500, \text{fluctuating regime}). \tag{8}$$

The transition between these two mass transfer regimes is observed around $Re \cong 100$–200, i.e. at the flow rate for which the inception of near-wall flow fluctuations is expected. The mass transfer coefficient measured in the flow cell is significantly higher than that observed in straight square channels. As seen in Figure 7 the experimental data are clearly above the lines representing the Lévêque equation (for laminar regime) [13]:

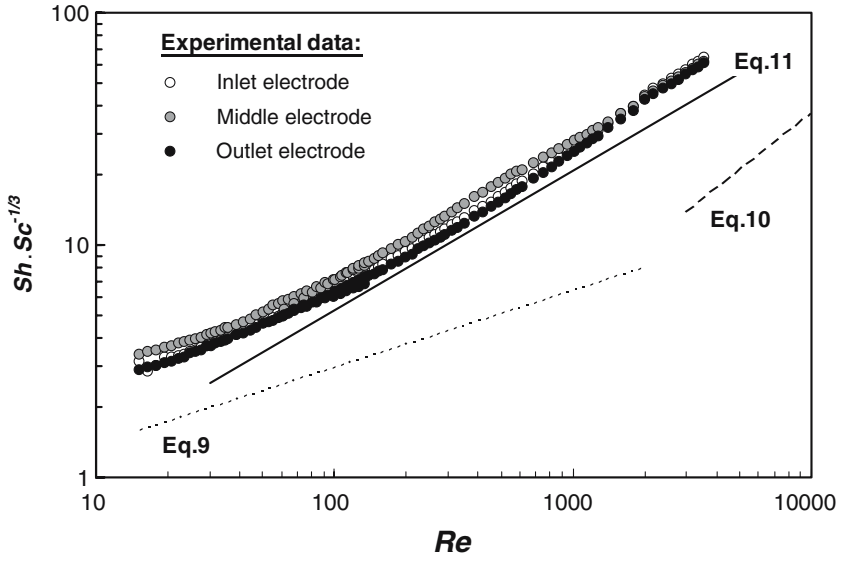

Fig. 7. Comparison of the measured wall mass transfer data with the correlations previously obtained for porous media and straight channels.

$$\mathrm{ShSc}^{-1/3} = 1.85\left(\frac{d_h}{l_e}\right)^{1/3} Re^{1/3} \tag{9}$$

and the equation obtained by the Chilton–Colburn analogy and cited by Coeuret and Storck [14] (for turbulent regime):

$$\mathrm{ShSc}^{-1/3} = 0.023 Re^{0.8} \tag{10}$$

For comparison, the classical correlation, which is proposed for mass transfer in fixed beds of spheres [15], is also shown in Figure 7. After transformation of the particle dimensionless numbers into those for pore and application of the capillary model for description of a microchannel network between individual spheres [16], the original Wakao correlation can be expressed in the form

$$\mathrm{ShSc}^{-1/3} = 0.33 Re^{0.6}. \tag{11}$$

This correlation is, especially for $Re > 200$, in relatively good agreement with the present mass transfer data (note the good agreement between the Reynolds number exponents in Equations 8 and 11). Consequently, from a mass transfer point of view, the studied flow cell can be compared to a porous medium rather than to a set of straight channels.

5. Conclusion

Electrodiffusion diagnostics have been proved to be a suitable experimental technique for the investigation of flow structure and mass transfer in a flow cell with crossing minichannels. The wall shear rate data provide information on the different flow regimes occurring. The flow is found to be laminar and stable only at low Reynolds numbers and the first flow fluctuations are observed at $Re \sim 200$. Under transitional flow conditions, the fluctuation rate increases rapidly and reaches a locally constant level at $Re \sim 1100$. This flow regimes delimitation is similar to that previously observed for porous media [11, 12]. However, even after fluctuation rate stabilization, the flow is still dominated by large coherent structures rather than by small turbulent vortices. The results of wall shear rate measurements provided by an array of microelectrodes demonstrate complex and unsteady flow conditions in the square channel sections, especially due to the flow redistribution at the crossings. From a mass transfer point of view, the studied flow configuration can also be compared to a porous medium rather than to a set of straight channels.

Acknowledgements

This work was partially supported by the Grant Agency of the Czech Republic under the project No. 101/04/0745 and by EC in the frame of the Marie Curie Training Sites programme HPMT-CT-2000-00074.

References

1. K.F. Jensen, *AIChE J.* **45** (1999) 2051.
2. M. Matlosz and J.M. Commenge, *Chimia* **56** (2002) 1.
3. G.L. Morini, *J. Therm. Sci.* **43** (2004) 651.
4. Z.X. Li, D.X. Du and Z.Y. Guo, *Microscale Thermophys. Eng.* **7** (2003) 253.
5. P.X. Jiang, M.H. Fan, G.S. Si and Z.P. Ren, *Int. J. Heat Mass Transfer* **44** (2001) 1039.
6. T.J. Hanratty and J.A. Campbell, Measurement of wall shear stress, in 'Fluid mechanics measurements' (edited by J.R. Goldstein), (Washington, Hemisphere, 1983) pp. 559.

7. V.E. Nakoryakov, A.P. Burdukov, O.N. Kashinsky and P.I. Geshev, 'Electrodiffusion method of investigation into the local structure of turbulent flows' (edited by V.E. Gasenko), (Novosibirsk, 1986) (in Russian).
8. C. Deslouis, O. Gil and B. Tribollet, *J. Fluid Mech.* **215** (1990) 85.
9. V. Sobolík, J. Tihon, O. Wein and K. Wichterle, *J. Appl. Electrochem.* **28** (1998) 329.
10. J. Tihon, V. Tovchigrechko, V. Sobolík and O. Wein, *J. Appl. Electrochem.* **33** (2003) 577.
11. D. Seguin, A. Montillet and J. Comiti, *J. Chem. Eng. Sci.* **53** (1998) 3751.
12. D. Seguin, A. Montillet and J. Comiti, *J. Chem. Eng. Sci.* **53** (1998) 3897.
13. M.A. Lévêque, *Ann. Mines* **12** (1928) 201.
14. F. Coeuret and A. Storck, *Eléments de génie électrochimique* (Technique et Documentation (Lavoisier), Paris, 1984), pp. 135.
15. N. Wakao and T. Funazkri, *Chem. Eng. Sci.* **33** (1978) 1375.
16. J. Comiti and M. Renaud, *Chem. Eng. Sci.* **44** (1989) 1539.